Submitted to WindPower 2013 to be held 5-8 May 2013 in Chicago, IL.

TWO-COMPONENT WIND FIELDS FROM SCANNING AEROSOL LIDAR AND MOTION ESTIMATION ALGORITHMS

Shane D. Mayor[1], Pierre Dérian[1,2], Christopher F. Mauzey[1], Tyson Henry[1], Etienne Mémin[2], Masaki Hamada[1], and Denton Scott[1]

[1] *California State University Chico, Chico, CA 95929, USA*

[2] *INRIA Rennes - Bretagne Atlantique, 35042 Rennes Cedex, FRANCE*

ABSTRACT

We report on recent developments and tests of an approach to measure the two-component horizontal wind field over areas of 10 to 20 square kilometers with spatial resolutions ranging from 100 m to 1 km and update rates of every 10 to 30 s. The approach employs a horizontally scanning, eye-safe, elastic backscatter aerosol lidar (the Raman-shifted Eye-safe Aerosol Lidar, or "REAL") and the application of numerical motion estimation algorithms to determine the velocity of a mixture of naturally occurring and anthropogenic aerosol features in the sequence of images that the lidar produces. Compared to Doppler lidars, which measure directly only a single component (the radial or "line-of-sight" component) of the flow, the technique that we report on provides a measurement of two velocity components. Our goal is to obtain the highest resolution wind fields over the largest areas possible with this technique and the hardware used may be scaled up to survey areas at longer ranges. We think this approach may have advantages for applications in wind energy—in particular, very short term wind forecasting and offshore wind resource assessments.

1. INTRODUCTION

Presently, the leading method to measure the wind with lasers is by the use of Doppler lidars [1; 2; 3; 4; 5]. These instruments are essentially interferometers that mix backscattered laser radiation from the atmosphere with a continuous sample of the radiation that was transmitted in order to obtain a beat note that is proportional to the frequency shift and caused by the wind-induced drift of aerosol particles. The technique is robust and highly accurate and gained much popularity in recent years, especially since compact and affordable systems have become commercially available. The technique to measure the frequency shift is known as optical heterodyne detection and it requires a high degree of coherence in the transmitted and backscattered laser radiation. However, the requirement for coherence places limitations on several important aspects of the system. For example, because the velocity measurement precision using this technique is related to laser pulse length, there is a tendency to use long pulses which reduce the range resolution of the data. Similarly, speckle diminishes the benefits of using larger telescope diameters which are advantageous to collect more signal and see farther.

Doppler lidars are also limited to a direct measurement of only the radial component of air motion (also often referred to as the *line-of-sight* component). This is only one of three components of air motion in the native spherical coordinate system of any radar or lidar. In order to obtain two or more components of air motion with Doppler lidar, one or more of several additional techniques must be employed. They include: (1) the carefully coordinated use of two or more Doppler systems separated by a significant distance (known as dual-Doppler) [6; 7; 8]; (2) the use of full or wide sector scans, the assumption of homogeneous flow, and curve fitting techniques to obtain vertical profiles of horizontal winds [9]; and (3) the use of numerical flow retrieval models [10; 11]. These methods either increase the cost and complexity of two-component wind measurements significantly or rely upon assumptions (e.g., horizontally homogeneous flow) that may not always be true.

In this paper, we report on research and development of a very different approach to obtain 2-component wind fields. The method is akin to the technique of *particle image velocimetry* (PIV) that is routinely used in laboratories to observe flow fields around objects for aerodynamic engineering and studies in fluid mechanics [12; 13]. PIV uses sequences of digital images of seeded flows and numerical motion estimation algorithms to derive vector flow fields. The seeds serve as a tracer of the fluid motion. Practicing PIV in the atmosphere is substantially more difficult because we cannot control the flow, and deliberate seeding with tracers, as is done in laboratory PIV, is not practical. Instead, we must rely on naturally occurring aerosols (particulate matter) and small-scale mixing to generate inhomogeneities in the aerosol field that we assume move with the flow. Anthropogenic aerosol features may also be present in the images. In addition, the visual signature of these aerosol perturbations evolve as they deform and are diffused, which further challenges the algorithms.

2. BACKGROUND

The largest efforts to measure the wind by aerosol lidar using a cross-correlation motion estimation algorithm were conducted by the University of Wisconsin-Madison [14; 15; 16; 17; 18; 19]. Other works include those by Japanese and Bulgarian researchers [20; 21]. Mayor and Eloranta [19] used the technique to measure offshore winds over the western edge of Lake Michigan during the 1997 Lake-Induced Convection Experiment

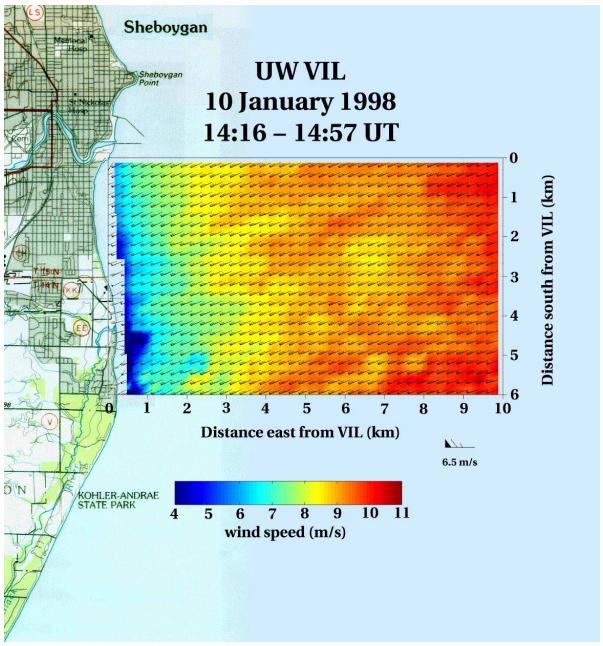

Figure 1: (Color required.) Mean offshore vector wind field derived from aerosol backscatter scans of the University of Wisconsin Volume Imaging Lidar (UW-VIL) during the 1997-1998 Lake-Induced Convection Experiment (Lake-ICE) using the cross-correlation technique. 41-minutes of cross-correlation functions were averaged. Vectors are spaced every 250 m. Color beneath the vectors represents wind speed ranging from about 4 m s^{-1} near the coast to $>$ 10 m s^{-1} at 10 km offshore. (From Mayor and Eloranta (2001) [19]).

(Lake-ICE) to validate numerical atmospheric simulations. They retrieved mean two-component vector wind fields with 250 m $\times$ 250 m resolution from the shore to 10 km offshore by averaging cross-correlation functions over periods of up to 41 minutes (see Fig. 1). Unfortunately, the lidar used was not eye-safe and the wind measurements were not validated. In the next sections of this paper, we describe an eye-safe elastic backscatter lidar system with similar capability, albeit reduced performance compared to the Wisconsin lidar, and our efforts to validate the winds derived from three different motion estimation algorithms.

3. RAMAN-SHIFTED EYE-SAFE AEROSOL LIDAR (REAL)

Based on the encouraging results of [19], the development of an eye-safe version of the University of Wisconsin Volume Imaging Lidar (UW-VIL) was started in 2001 at the National Center for Atmospheric Research (NCAR) in Boulder, Colorado. The effort resulted in the Raman-shifted Eye-safe Aerosol Lidar (REAL, see Fig. 2, [22; 23; 24; 25]). In comparison to the UW-VIL, the REAL operates at 1.54 microns wavelength instead of 1.064 microns. It also has significantly reduced transmit

Figure 2: The NSF/NCAR Raman-shifted Eye-safe Aerosol Lidar (REAL) at California State University Chico.

power: 10 Hz instead of 100 Hz and 170 mJ per pulse instead of 400 mJ. This is a reduction in average transmit power by a factor of more than 20. However, the reduction is not for eye-safety. Much more energy could be transmitted safely at this longer wavelength. The reduction is due to challenges with producing laser pulses with suitable characteristics (energy, pulse length, divergence) for lidar at 1.5 microns wavelength. A path does exist for increasing the pulse energy and pulse rate at 1.5 microns wavelength. Indeed, Spuler and Mayor [25] demonstrated 390 mJ at 50 Hz in the laboratory.

Wavelength	1.543 microns
Pulse energy	170 mJ
Pulse rate	10 Hz
Pulse duration	6 ns
Beam diameter at BSU	66 mm (1/e^2 points)
Beam divergence	0.12 mrad (half-angle)
Telescope dia.	40 cm
Receiver FOV	0.54 mrad
Digitizer speed	100 MHz
Digitizer range	14 bits
Detector type	200-μm InGaAs APD

Table 1: Specifications of the NSF/NCAR REAL.

The REAL is a direct-detection elastic backscatter lidar. It is distinct from other aerosol lidars in that it operates at 1.54-microns wavelength and safely transmits energetic infrared laser pulses. The laser pulses are generated by use of a commercially-available Nd:YAG laser and stimulated Raman scattering in an injection-seeded high-pressure gas cell. Table 1 lists the specifications of the original NSF/NCAR REAL. Under most conditions, the system is capable of generating useful backscatter (i.e., signal-to-noise ratio (SNR) ranging from more than 100 at 500 m to 10 at 3 km) to ranges of 3–5 km from each laser pulse. No averaging, over space or time, of the backscatter returns is necessary. As an example, 60-degree wide horizontal scans require 10–30 s to collect depending on the scan rate and desired angular resolution, and are composed of 100 to 300 radial backscat-

Figure 3: The NSF/NCAR REAL was located exactly 1.61 km north of a 30-m tall tower during the 2007 CHATS field experiment near Dixon, CA. 2-component wind vectors were calculated using the cross-correlation technique for image subsets outlined by the 4 concentric white squares.

ter arrays. Each backscatter array contains thousands of samples spaced at 1.5 m intervals in range. A high-pass median filter is applied to each array to remove unwanted artifacts and large-scale features caused by attenuation. These filtered data, in polar form, are interpolated to a Cartesian grid, typically with 10 m $\times$ 10 m spacing. The motion estimation algorithms described in Section 4 operate on the Cartesian arrays.

4. THREE ALGORITHMS AND COMPARISON OF RESULTS WITH ANEMOMETER DATA

From mid-March through early June of 2007, the NSF/NCAR REAL was deployed in Dixon, California, for the Canopy Horizontal Array Turbulence Study (CHATS) [26]. The REAL was located 1.6 km north of a 30-m instrumented tower. The tower was located in a large walnut orchard (mean tree top height about 10 m AGL) in order to study the effect of an idealized forest canopy on atmospheric fluxes. The REAL collected nearly-horizontal scans (slope of 8.6 m per 1000 m) that intersected the tower at about 20 m AGL. Sonic anemometers on the tower near the height of the scan surface were used to provide in situ wind measurements for comparison and validation. Fig. 3 shows the experimental arrangement. The resulting data set is very large. For brevity, we present results from just one 4 hour period here. The period is interesting because a density current front passed over the experimental area causing the wind direction to reverse. A detailed description of these fronts can be found in [27]. Two-component winds during the period were calculated by three different numerical methods: cross-correlation (Section 4.1), optical-flow (Section 4.2), and wavelet-based optical flow (Section 4.3). Although the two investigated families of optical flow methods share a similar framework, they are conceptually very different. Both approaches combine a *data model*, that link image data to the underlying motion, and a *regularizer* to close the otherwise under-constrained estimation problem. The data model usually comes from a brightness consistency assumption – that is to say, the brightness, in the image sequence, of a given feature remains identical as the feature is advected by the flow. Regularizers generally enforce some spatial smoothing of the estimated motion.

Cross-correlations perform a set of *independent, local* measurements on small subregions of the image, assuming a constant motion over the considered windows. It finds an efficient implementation thanks to the Fourier transform, and can be easily parallelized due to the independence of measures. Optic flow approaches, on the contrary, look for a motion that minimizes a *global* functional defined over the whole image domain. They are widely used in robotic navigation (visual odometry), video surveillance, stereo reconstruction, autonomous navigation, flight control, and video compression. A great advantage of these methods lies in their flexibility. Indeed, the data model and the regularizer can be designed to take into account the specificities of the investigated images and the dynamics of the motion, whereas cross-correlations are limited to a single data model (actually, the cross-correlations itself) and regularizer (the constant motion assumption). As such, fluid-dedicated approaches have been suggested [28]. The drawbacks are their increased computational burden, as they involve many more unknowns that cross-correlations, and their poor ability to cope with large apparent displacements requires the use of an incremental, multiscale estimation scheme. Most recently, the wavelet-based optical flow benefits from wavelet bases properties to offer a "naturally" multiscale approach, as well as efficient implementations of various regularizer [29; 30].

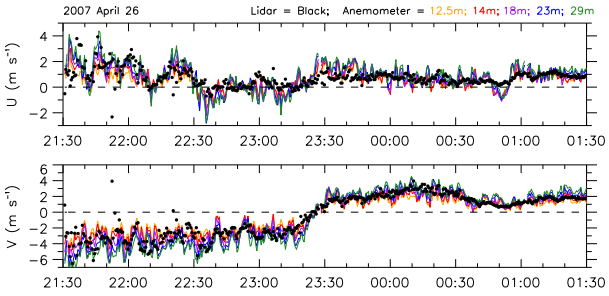

Figure 4: Time-series of wind components (u is east-west and v is north-south) from the cross-correlation technique (black dots) and tower-mounted sonic anemometers at various heights (colored lines) during the passage of a density current front on 26 April 2007.

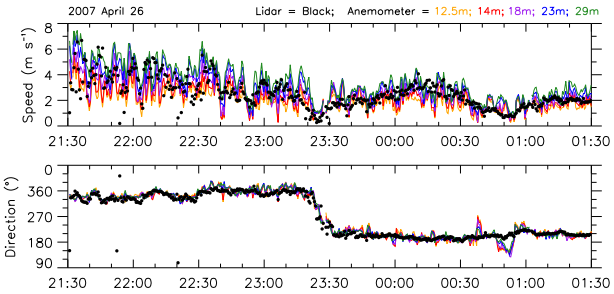

Figure 5: Same data as in Fig. 4, expect plotted as speed (top) and direction (bottom).

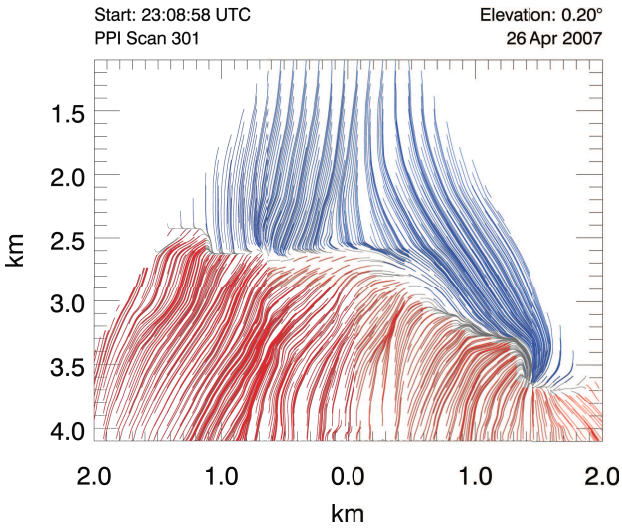

Figure 6: Streamlines through the 2-component vector wind field that resulted from the application of the cross-correlation technique to a pair of elastic backscatter images when a density current front intersected the scan area. Streamlines are colored according to the v-component with blue indicating northerly flow north of the front and red indicating southerly flow south of the front.

4.1. Cross-correlation

Cross-correlation (phase correlation) is the most widely-used algorithm for retrieval of vector flow fields from fluid motion image sequences. A recent paper by Mayor et al. [31] describes in detail the performance of a cross-correlation algorithm by comparing the resulting vector components with those from tower-mounted sonic anemometers. The algorithm, as applied to aerosol lidar data, is described by Schols and Eloranta [18]. Over 180,000 pairs of vectors were compared from 75 days of data during CHATS. For each vector comparison, turbulent kinetic energy (TKE), wind speed, mean signal-to-noise ratio (SNR), and maxima of the cross-correlations functions were recorded. In general, it was found that improved correlations of vector components existed at night when the wind speeds and TKE were low. Similarly, the correlations improved with increasing SNR and CCF maxima. Although the correlation between the two types of measurements tended to be poor over short-periods during the day, the means were often in good agreement.

4.2. Optical flow

The cross-correlation technique is capable of providing useful results, but it requires adequate image content in the interrogation window to produce a quality vector representative of that area. In 2010, we applied an optical flow algorithm described by Corpetti et al. [28] to a few hours of the REAL data from CHATS and compared the results with the sonic anemometer data [32]. In general, very good agreement was found and it was a step in the right direction to see a solution that provided a vector at every pixel without unrealistic excursions from noise. The lack of noise in the solutions made it possible to see physically realistic kinematic quantities such as divergence and vorticity in the flow fields. (See color images in right column of Fig. 8). [1] However, this specific implementation of optical flow provided fields that were judged by most potential users of the results as smoother than desired. This work confirmed our hypothesis that optical flow has clear merits over cross-correlation for lidar data, and inspired the work described in the next section.

[1] Mayor and Eloranta [19] also showed divergence and vorticity, but it was computed from mean flow fields that required many minutes to acquire. Here, divergence and vorticity were calculated from a flow field that required just two scans which took only 17 s to acquire.

4.3. Wavelet-based optical flow

The flow fields shown in Figs. 9 and 10 were computed with the latest wavelet-based motion estimation algorithm. Details of the approach can be found in [29; 30]. These figures present time-series comparisons with sonic anemometer data (direction and speed in Fig. 9) and streamlines corresponding to one estimated velocity field, superimposed on one of the input lidar images used by the algorithm. Apart from the noticeable aerosol features (in red and dark blue), these images are rather noisy (when compared to images used in PIV). The implementation of a "robust" estimation method, using so-called M-estimators, was therefore necessary to process this data. These examples are very early results, as up to now the mentioned wavelet-based approach has been successfully tested on more classical, much less noisy particle or scalar transport images. Yet it illustrates how the algorithm is capable of handling a rather complex situation (heavy convergence due to the moving front) from a small number of tracers, and results in coherent estimates. In the future, we plan to adapt the method to the specificities of lidar images, by enforcing furthermore the robustness to noise and developing a lidar-dedicated data model.

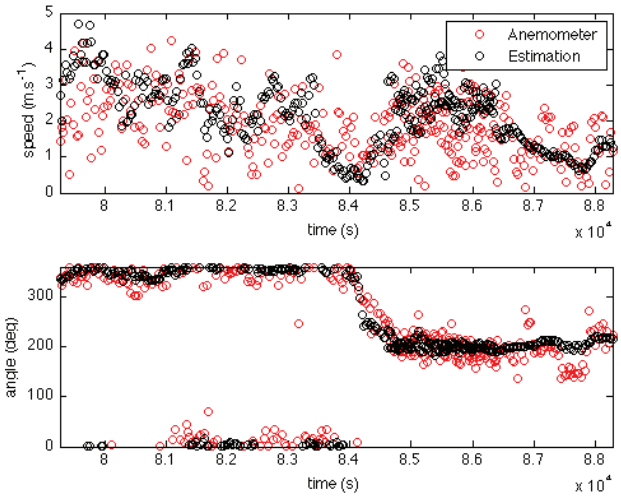

Figure 7: Time-series of wind speed (top) and direction (bottom) from an optical flow technique (black circles) and sonic anemometer (red circles) during the passage of a density current front on 26 April 2007. The timespan shown is about 2.5 hours.

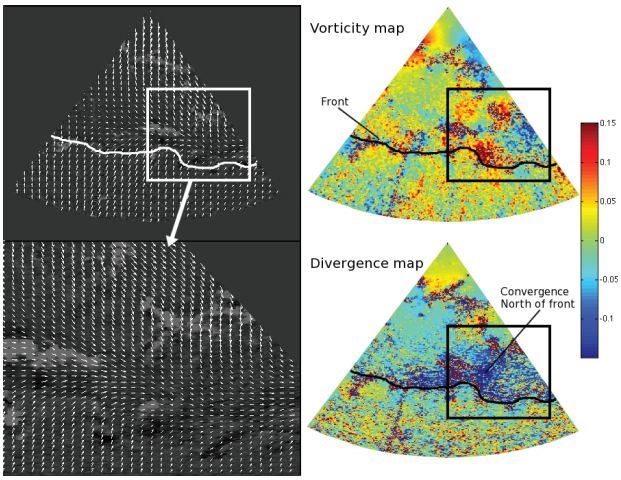

Figure 8: Vector flow fields (left) and kinematic quantities in color (right, vorticity in top and divergence in bottom) resulting from the application of an optical flow algorithm to a pair of scans from the REAL during the passage of a density current front on 26 April 2007.

5. RECENT SYSTEM IMPROVEMENTS

5.1. Hardware improvements

We are currently implementing several hardware upgrades in the NSF/NCAR REAL to improve optical efficiency and reliability of the instrument. Our goal in this area is to reveal the smallest possible changes in aerosol backscattering over the largest areas and longest ranges possible. The activities include re-routing the laser beam

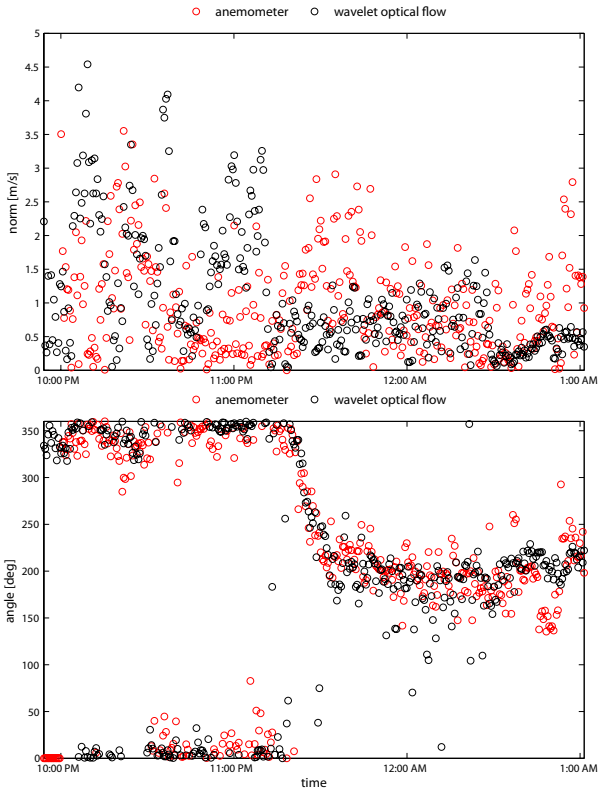

Figure 9: Time-series of wind speed (top) and direction (bottom) from a wavelet-based optical flow technique (black circles) and sonic anemometer (red circles) during the passage of a density current front on 26 April 2007.

within the transmitter subsystem, replacing several kinematic mirror mounts with gimbal mirror mounts, and fabricating an improved positive-pressure enclosure around the transmitter subsystem. In addition, we are procuring gas-fusion beam-steering unit (BSU) mirrors with enhanced gold coatings for an average reflectivity per mirror greater than 99.6%. We estimate the old mirrors to have reflectivity between 90 and 96%. Given two BSU mirrors and two passes (transmit and receive), we expect to reduce optical losses in the BSU alone from 15–34% to less than 2% [33]. These improvements will enable better performance in terms of increased SNR and range and more durability for long-term operation.

5.2. Control system

Wind monitoring requires long, uninterrupted periods of measurement. Continuous and unattended operation of a high energy laser requires a control system that can sense potential problems and take automatic action if necessary to protect the system from damaging itself. A control system can also stabilize transmitter power by periodically adjusting laser flashlamp voltage and reminding operators of the need for maintenance (e.g., flashlamp

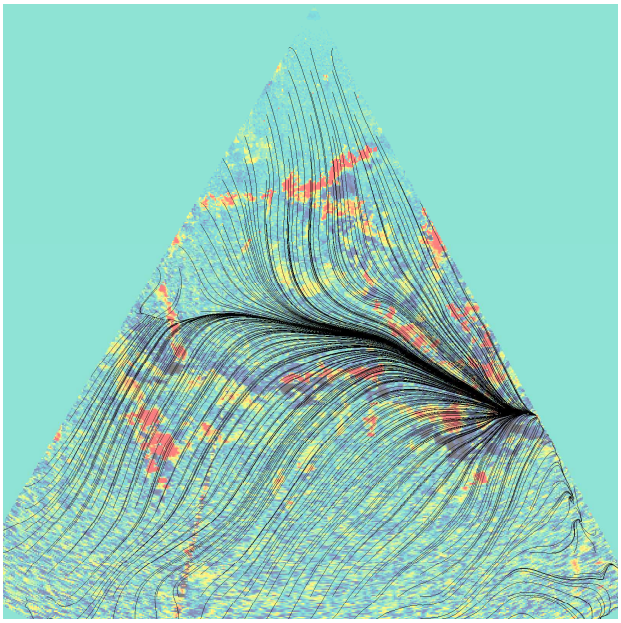

Figure 10: Streamlines through a 2-component vector flow field that resulted from application of a wavelet-based optical flow algorithm to a pair of scans from the REAL during the passage of a density current front on 26 April 2007.

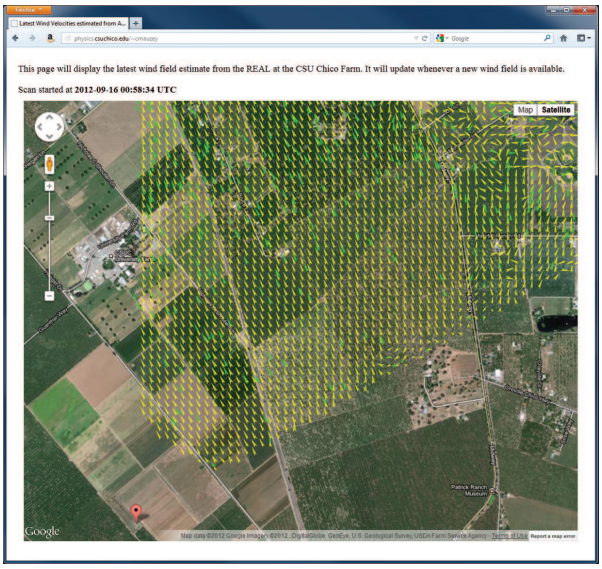

Figure 11: A web-application enables users to view the most recent two-component vector wind field overlaid on a Google Earth map within seconds after the data are collected. The vectors are computed in real-time by an Nvidia Tesla GPU and the flow fields are uploaded to a database on a server in the Department of Physics at California State University Chico.

changes[2]). A lidar control system, written in Labview, has been developed and is currently being tested. The system senses laser beam characteristics, temperatures, pressures, and motion, and either (1) shuts down gracefully; (2) makes small adjustments; or (3) informs operators of changes.

One potential application of this lidar system is offshore wind assessment. The instrument could be installed on the ground near the shore and scan horizontally with the beam directed over the water. (As was done for the data shown in Fig. 1.) Precise and accurate measurement of the altitude of the lidar beam above the water is important. Small tips and tilts of the lidar platform result in large changes in the altitude of the beam offshore. For example, rolling the horizontal deck of the trailer by 1 mm would displace the beam over 4 m altitude at 10 km range. To solve this problem, we invested in two tiltmeters each employing gravity-referenced electrolytic tilt transducers with 0.001-degree resolution. At the time of this writing we are simply recording this data to study the stability of our platform. However, in the future, this information could be supplied to the control system and the elevation angle of the BSU could be adjusted in real-time to maintain constant altitude of the scan offshore.

[2]Currently, laser flashlamps must be replaced every 20M-30M pulses. The replacement requires less than 30 minutes of downtime.

5.3. Real-time winds

We recently completed development of the ability to compute vector wind fields in real-time using the cross-correlation technique. The algorithm requires many computationally intensive operations such as sorting for filtering, interpolation for gridding, and fast-Fourier transforms for calculation of the cross-correlation functions. Traditional computer programs do not typically utilize the multicore power of modern CPUs efficiently. Furthermore, graphical processing units (GPUs) can dramatically accelerate the execution of software applications by distributing the computation across hundreds of smaller processors. This is especially true for image blocks with a large number of pixels. Therefore, the software application was written to take advantage of these architectures. Upon completion of the calculation of one vector flow field for one pair of scans, the vector flow field is transmitted to an SQL database that can be read by a web-application to enable users to display the flow fields in near-real-time from anywhere with an internet connection.

6. A MORE COMPACT, 20 HZ REAL

As of 3 September 2012, the CSU Chico Atmospheric Lidar Research Group is now home to a second REAL thanks to an equipment transfer from the Pentagon Force Protection Agency (PFPA). The instrument was recently received from PFPA through the US National Science Foundation (NSF) and the National Center for Atmo-

Figure 12: A more compact REAL with twice the pulse-rate of the original REAL is now available. This system is approximately 2.5 m wide by 3 m long.

spheric Research (NCAR) for use in atmospheric research and education. The second-generation REAL was built by ITT Corp. and is considerably smaller than the original REAL that has been at Chico State since 2008. The CSU Chico Atmospheric Lidar Research Group will maintain the instrument, along with its larger elder brother, and use them both for research related to wind energy, aerosols, air quality, and other topics in meteorology.

7. CONCLUSIONS AND FUTURE PLANS

Further assessment of the integrity of the velocities from the two optical flow algorithms could be performed by making point by point comparisons with the sonic anemometer data (as was done for the cross-correlation results) and comparing the distributions of velocity component differences. In addition, time-series analysis may reveal the noise levels in the results. However, the REAL scans from CHATS data set have several problems which make the comparison and anaysis challenging. These include periodic unequal time separation of the lidar vectors (due to an idiosyncrasy in the data collection software at that time) and occasional hard target reflections in the backscatter images from the tower. Finally, the lidar trailer was not as stable as it should have been during CHATS resulting in variation and some uncertainty of the height of the scan surface at the tower location.

We plan to operate the REAL at California State University Chico for a 6-month period starting in June of 2013 and compare retrieved winds with those from a compact Doppler lidar. The evaluation will be performed at altitudes of 50 to 150 m AGL in order to provide more data on the performance of this technique at altitudes swept by large wind turbines. All of the experimental deficiencies encountered in CHATS will be addressed. In the future, we would like to deploy one of the REALs at a coastal location to evaluate its performance in a marine environment.

The instruments currently available are suited for wind measurements between 500 m and 3–5 km horizontal range. We note that the technology can be scaled up to be effective at longer ranges. For example, by increasing the telescope diameter from 40 cm to 60 cm, a doubling in receiver collection area will be achieved. (Increasing the telescope diameter would require larger BSU optics, but this can be done.) Similarly, the transmitted pulse energy could be increased substantially. Eye-safety could be maintained by increasing the transmit beam diameter to match the current energy density within the beam. Nd:YAG lasers capable of delivering 3 J of pump energy at 10 Hz pulse rate are commercially available. With 25% conversion efficiency in the Raman-shifter, this could produce 750 mJ at 1.54 microns wavelength.

ACKNOWLEDGMENTS

This paper is based upon research supported by the US National Science Foundation Physical and Dynamic Meteorology program under Grants 0924407, 1104342, and 1228464. We also thank our collaborators at the National Center for Atmospheric Research.

REFERENCES

1. Menzies, R. T. and Hardesty, R. M. 1989: Coherent Doppler lidar for measurements of wind fields. *Proc. IEEE.*, **77**, 449–462.
2. Post, M. J. and Cupp, R. E. 1990: Optimizing a pulsed Doppler lidar. *Appl. Optics*, **29**, 4115–4158.
3. Henderson, S. W., Hale, C. P., Magee, J. R., Kavaya, M. J., and Huffaker, A. V. 1991: Eye-safe coherent laser radar system at 2.1 micron using Tm,Ho:YAG lasers. *Opt. Lett.*, **16**, 773–775.
4. Grund, C. J., Banta, R. M., George, J. L., Howell, J. N., Post, M. J., Richter, R. A. and Weickman, A. M. 2001: High-resolution Doppler lidar for boundary layer and cloud research. *J. Atmos. Ocean. Technol.*, **18**, 376–393.
5. Pearson, G., Davies, F., and Collier, C. 2009: An analysis of the performance of the UFAM pulsed Doppler lidar for observing the boundary layer. *J. Atmos. Ocean. Technol.*, **26**, 240–250.
6. Newsom, R. K., Ligon, D., Calhoun, R., Heap, R., Cregan E., and Princevac, M. 2005: Retrieval of Microscale wind and temperature fields from single- and dual-Doppler lidar data. *J. Appl. Meteor.*, **44**, 1324–1345.
7. Newsom, R.K., Calhoun, R., Ligon, D., and Allwine, K. J. 2008: Linearly organized turbulence structures observed over a suburban area by dual-Doppler lidar. *Bound. Layer Meteor.*, **127**, 111–130.

8. Hill, M., Calhoun, R., Fernando, H. J. S., Wieser, A., Dörnbrack, A., Wiessmann, M., Mayr, G., and Newsom, R. K. 2010: Coplanar Doppler lidar retrieval of rotors from T-REX. *J. Atmos. Sci.*, **67**, 713–729.
9. Browning, K. A. and Wexler, R. 1968: The determination of kinematic properties of a wind field using a Doppler radar. *J. Appl. Meteor.*, **7**, 105–113.
10. Newsom, R. K. and Banta, R. M. 2004: Assimilating coherent Doppler lidar measurements into a model of the atmospheric boundary layer. Part I: Algorithm development and sensitivity to measurement error. *J. Atmos. Ocean. Technol.*, **21**, 1328–1345.
11. Newsom, R. K. and Banta, R. M. 2004: Assimilating coherent Doppler lidar measurements into a model of the atmospheric boundary layer. Part II: Sensitivity analyses. *J. Atmos. Ocean. Technol.*, **21**, 1809–1824.
12. Adrian, R. J. and Westerweel, J. *Particle Image Velocimetry*. Cambridge University Press, New York, 2011.
13. Raffel, M., Willert, C., Wereley, S. and Kompenhans, J. *Particle Image Velocimetry* Second Edition. Springer-Verlag, Berlin, 2007.
14. Eloranta, E. W., King, J. M., and Weinman, J. A. 1975: The determination of wind speeds in the boundary layer by monostatic lidar. *J. Appl. Meteor.*, **14**, 1485–1489.
15. Sroga, J. T., Eloranta, E. W., and Barber, T. 1980: Lidar measurements of wind velocity profiles in the boundary layer. *J. Appl. Meteor.*, **19**, 598–605.
16. Kunkel, K. E., Eloranta, E. W., and Weinman, J. 1980: Remote determination of winds, turbulence spectra and energy dissipation rates in the boundary layer from lidar measurements. *J. Atmos. Sci.*, **37**, 978–985.
17. Hooper, W. P. and Eloranta, E. W. 1986: Lidar measurements of wind in the planetary boundary layer: the method, accuracy and results from joint measurements with radiosonde and kytoon. *J. Clim. Appl. Meteor.*, **25**, 990–1001.
18. Schols, J. L. and Eloranta, E. W. 1992: The calculation of area-averaged vertical profiles of the horizontal wind velocity from volume imaging lidar data. *J. Geophys. Res*, **97**, 18395–18407.
19. Mayor, S. D. and Eloranta, E. W. 2001: Two-dimensional vector wind fields from volume imaging lidar data. *J. Appl. Meteor.*, **40**, 1331–1346.
20. Sasano, Y., Hirohara, H., Yamasaki, T., Shimizu, H., Takeuchi, N., and Kawamura, T. 1982: Horizontal wind vector determination from the displacement of aerosol distribution patterns observed by a scanning lidar. *J. Appl. Meteor.*, **21**, 1516–1523.
21. Kolev, I., Parvanov, O., and Kaprielov, B. 1988: Lidar determination of winds by aerosol inhomogeneities: motion velocity in the planetary boundary layer. *Appl. Optics*, **27**, 2524–2531.
22. Mayor, S. D. and Spuler, S. M. 2004: Raman-shifted Eye-safe Aerosol Lidar. *Appl. Optics*, **43**, 3915–3924.
23. Spuler, S. M. and Mayor, S. D. 2005: Scanning Eye-safe Elastic Backscatter Lidar at 1.54 microns, *J. Atmos. Ocean. Technol.*, **22**, 696-703.
24. Mayor, S. D., Spuler, S. M., Morley, B. M., and Loew, E. 2007: Polarization lidar at 1.54-microns and observations of plumes from aerosol generators. *Opt. Eng.*, **46**, DOI: 10.1117/12.781902.
25. Spuler, S. M. and Mayor, S. D. 2007: Raman shifter optimized for lidar at 1.5-micron wavelength. *Appl. Optics*, **46**, 2990-2995.
26. Patton, E. G., et al. 2011: The Canopy Horizontal Array Turbulence Study (CHATS) *Bull. Amer. Meteorol. Soc.*, **92**, 593-611.
27. Mayor, S. D. 2011: Observations of seven atmospheric density current fronts in Dixon, California. *Mon. Wea. Rev.*, **139**, 1338-1351.
28. Corpetti, T., Mémin, E., and Perez, P. 2002: Dense estimation of fluid flows. *IEEE Trans. Pattern Analysis Machine Intelligence*, **24**, 365–380.
29. Dérian, P., Héas, P., Herzet, C., and Mémin, E. 2012: Wavelets and optical flow motion estimation. Submitted to NM-TMA, under minor revision.
30. Kadri-Harouna, S., Dérian, P., Héas, P., and Mémin, E. 2012: Divergence-free wavelets and high order regularization. Submitted to IJCV, under minor revision.
31. Mayor, S. D., Lowe, J. P., and Mauzey, C. F. 2012: Two-component horizontal aerosol motion vectors in the atmospheric surface layer from a cross-correlation algorithm applied to elastic backscatter lidar data. *J. Atmos. Ocean. Technol.*, In press.
32. Dérian, P., Héas, P., Mémin, E., Mayor, S. D. 2010: Dense motion estimation from eye-safe aerosol lidar data. 25th Int. Laser Radar Conf. Paper S3O-04. **1**, 377-380.
33. Mayor, S. D., Petrova-Mayor, A., Wortley, R. W. Hofstadter, D. S., Spuler, S. M., and Ranson, J. 2011: Gas-fusion mirrors for atmospheric lidar. JTuA19. Frontiers in Optics. Optical Society of America.